

Simultaneous estimation of noise variance and number of peaks in Bayesian spectral deconvolution

Satoru Tokuda¹, Kenji Nagata²³, and Masato Okada^{14*}

¹*Department of Complexity Science and Engineering, The University of Tokyo, Kashiwa, Chiba 277-8561, Japan*

²*Artificial Intelligence Research Center, AIST, Koto, Tokyo 135-0064, Japan*

³*PRESTO, Japan Science and Technology Agency, Kawaguchi, Saitama 332-0012, Japan*

⁴*RIKEN Brain Science Institute, Wako, Saitama 351-0198, Japan*

Heuristic identification of peaks from noisy complex spectra often leads to misunderstanding physical and chemical properties of matter. In this paper, we propose a framework based on Bayesian inference, which enables us to separate multi-peak spectra into single peaks statistically and is constructed in two steps. The first step is estimating both noise variance and number of peaks as hyperparameters based on Bayes free energy, which generally is not analytically tractable. The second step is fitting the parameters of each peak function to the given spectrum by calculating the posterior density, which has a problem of local minima and saddles since multi-peak models are nonlinear and hierarchical. Our framework enables escaping from local minima or saddles by using the exchange Monte Carlo method and calculates Bayes free energy. We discuss a simulation demonstrating how efficient our framework is and show that estimating both noise variance and number of peaks prevents overfitting, overpenalizing, and misunderstanding the precision of parameter estimation.

1. Introduction

Spectroscopy is at the heart of all sciences concerned with matter and energy. An electromagnetic spectrum of matter indicates the electronic states and kinetics of atoms depending on each energy region. The quantum nature of spectra is approximately reduced to the sum of unimodal peaks (such as Lorentzian peaks, Gaussian peaks, and their convolutions), whose centers are the energy levels from the semiclassical viewpoint.¹⁾ The peak intensity is proportional to both the population density of the atoms or molecules and their transition probabili-

*okada@k.u-tokyo.ac.jp

ties. The Lorentzian peak width indicates the lifetime of the eigenstate due to the time-energy uncertainty relation. The Gaussian peak width indicates the Doppler effect caused by the kinetics of atoms and depends on temperature. These pieces of information about the electronic states or kinetics of atoms are obtained by identifying peaks from spectra.

It is generally a difficult problem to distinguish each peak from noisy spectra with overlapping peaks. The simplest solution is least squares fitting by using a gradient method.²⁾ This type of method has a drawback in that fitting parameters are often trapped to a local minimum or a saddle whenever there is another global minimum in the parameter space. In the first place, the number of peaks is not always known in practice. Bayesian inference, by using a Markov chain Monte Carlo (MCMC) method, provides a superior solution.^{3–10)} Though the Bayesian framework enables us to estimate the number of peaks, MCMC methods generally have the limitation of local minima and saddles. Nagata et al. reported⁶⁾ that the exchange Monte Carlo method¹¹⁾ (or parallel tempering¹²⁾) can prevent local minima or saddles efficiently and provide more accurate estimation than the reversible jump MCMC method¹³⁾ and its extension.¹⁴⁾

We constructed a Bayesian framework for estimating both noise variance and number of peaks from spectra with white Gaussian noise by expanding the previous framework by Nagata et al.⁶⁾ Noise variance and number of peaks are respectively estimated by hyperparameter optimization and model selection. These estimations are carried out by maximizing a function called marginal likelihood,^{15–17)} which is a conditional probability of observed data given noise variance and the number of peaks in our framework. We provide a straightforward and efficient scheme that calculates this bivariate function by using the exchange Monte Carlo method. We also demonstrated our framework through simulation. We show that estimating both noise variance and number of peaks prevents overfitting, overpenalizing, and misunderstanding the precision of parameter estimation.

2. Framework

2.1 Models

An observed spectrum $y \in \mathbb{R}$ is represented by the sum $f(x; w)$ of single peaks $\phi_k(x; \mu_k, \rho_k)$ and additive noise ε as follows:

$$y = f(x; w) + \varepsilon, \quad (1)$$

$$f(x; w) = \sum_{k=1}^K a_k \phi_k(x; \mu_k, \rho_k), \quad (2)$$

$$\phi_k(x; \mu_k, \rho_k) = \exp\left(-\frac{\rho_k}{2}(x - \mu_k)^2\right), \quad (3)$$

where $x \in \mathbb{R}$ denotes energy, frequency or wave number depending on the case. The parameter set is $w = \{a_k, \mu_k, \rho_k\}_{k=1}^K$, where $a_k \geq 0$, $\mu_k \in \mathbb{R}$ and $\rho_k^{-1/2}(\rho_k \geq 0)$ for each k are respectively the intensity, energy level, and peak width. The Gaussian function $\phi_k(x)$ for each k should be replaced with other parametric functions, such as Lorentzian or Voigt, depending on the case.^{1, 18, 19)} If the peaks $\phi_k(x)$ are symmetric function for all k (i.e. these values depend only on the distance from each center), the function $f(x; w)$ is called a radial basis function network in the neural network and related fields.^{6, 20)} This is the junction of the spectral data analysis and singular learning theory.²¹⁾ If the additive noise ε is supposed to be zero-mean Gaussian with a variance $b^{-1} \geq 0$, the statistical model of the observed spectrum is represented by a conditional probability as follows:

$$p(y | x, w, b) = \sqrt{\frac{b}{2\pi}} \exp\left(-\frac{b}{2}(y - f(x; w))^2\right), \quad (4)$$

where y is taken as a random variable. This Gaussian distribution $p(y | x, w, b)$ is valid if the thermal noise is dominant. The parameter set w is also regarded as a random variable from the Bayesian viewpoint. The probability density function of w , called the *prior* density, is heuristically modeled as follows:

$$\varphi(w | K) = \prod_{k=1}^K \varphi(a_k) \varphi(\mu_k) \varphi(\rho_k), \quad (5)$$

$$\varphi(a_k) = \kappa \exp(-\kappa a_k), \quad (6)$$

$$\varphi(\mu_k) = \sqrt{\frac{\alpha}{2\pi}} \exp\left(-\frac{\alpha}{2}(\mu_k - \mu_0)^2\right) \quad (7)$$

$$\varphi(\rho_k) = \nu \exp(-\nu \rho_k), \quad (8)$$

where κ , μ_0 , α , and ν are hyperparameters. This prior density modeling is a special case of that by Nagata et al.⁶⁾ Equation (6) promotes non-negativity and sparseness as physical constraints. Equation (7) is regarded as almost flat prior density if α is sufficiently small. Equation (8) imposes non-negativity. These prior density models can be replaced with any other model without loss of generality in our framework.

2.2 Bayesian formalization

The conditional probability density function of w given samples $D = \{X_i, Y_i\}_{i=1}^n$ is represented by Bayes' theorem as follows:

$$p(w | D, K, b) = \frac{1}{Z_n(K, b)} \prod_{i=1}^n p(Y_i | X_i, w, b) \varphi(w | K) \quad (9)$$

$$= \frac{1}{\tilde{Z}_n(K, b)} \exp(-nbE_n(w)) \varphi(w | K), \quad (10)$$

$$Z_n(K, b) = \int dw \prod_{i=1}^n p(Y_i | X_i, w, b) \varphi(w | K), \quad (11)$$

$$\tilde{Z}_n(K, b) = \left(\frac{2\pi}{b}\right)^{\frac{n}{2}} Z_n(K, b), \quad (12)$$

$$E_n(w) = \frac{1}{2n} \sum_{i=1}^n (Y_i - f(X_i; w))^2, \quad (13)$$

where the functions $p(w | D, K, b)$ and $Z_n(K, b)$ are respectively called the *posterior* density and marginal likelihood. Note that the function $Z_n(K, b) = p(D | K, b)$ is a probability density but $\tilde{Z}_n(K, b)$ is not. Bayes free energy $F_n(K, b)$ is defined as follows:

$$F_n(K, b) = -\log Z_n(K, b) \quad (14)$$

$$= b\tilde{F}_n(K, b) - \frac{n}{2}(\log b - \log 2\pi), \quad (15)$$

$$\tilde{F}_n(K, b) = -\frac{1}{b} \log \tilde{Z}_n(K, b). \quad (16)$$

Note that Nagata et al. regarded $b\tilde{F}_n(K, b)$ as Bayes free energy for the sake of convenience⁶⁾ since noise variance is treated as a known constant. The partial derivative of $F_n(K, b)$ with respect to variable b is obtained as follows:

$$\frac{\partial F_n}{\partial b} = n \left(\langle E_n(w) \rangle_b - \frac{1}{2b} \right), \quad (17)$$

where $\langle \cdots \rangle_b$ denotes the posterior mean over the density $p(w | D, K, b)$. The optimal value of b , which minimizes $F_n(K, b)$ (or maximizes $Z_n(K, b)$), is achieved by setting the right side of Eq. (17) to zero as follows:

$$\langle E_n(w) \rangle_b = \frac{1}{2b}. \quad (18)$$

Then there exists $b > 0$ such that Eq. (18) is satisfied; however, the optimal b and $F_n(K, b)$ for our model are not analytically derived.

2.3 Monte Carlo procedure and Bayes free energy calculation

Practically, we sample w from $p(w \mid D, K, b)$ by using the exchange Monte Carlo method¹¹⁾ (or parallel tempering¹²⁾) and calculate $F_n(K, b)$. The target density is a joint probability density as follows:

$$p\left(\{w\}_{l=1}^L \mid D, K, \{b_l\}_{l=1}^L\right) = \prod_{l=1}^L p(w_l \mid D, K, b_l), \quad (19)$$

where b_l is set as $0 = b_1 < b_2 < \dots < b_L = b_{max}$. Each density $p(w_l \mid D, K, b_l)$ is called a *replica*. Note that variable b is replaced with inverse temperature β of Nagata et al.'s formulation.⁶⁾ Variable b works as quasi inverse temperature and varies the substantial support of the posterior density $p(w \mid D, K, b)$. The state exchange between high- and low-temperature replicas prompts the escape from local minima or saddles in the parameter space. The sampling procedure includes the two following steps.

- State update in each replica

Simultaneously and independently update state w_l subject to $p(w_l \mid D, K, b_l)$ by using the Metropolis algorithm.²²⁾

- State exchange between neighboring replicas

Exchange states w_l and w_{l+1} at every step subject to the probability $u(w_{l+1}, w_l, b_{l+1}, b_l)$ as follows:

$$u(w_{l+1}, w_l, b_{l+1}, b_l) = \min(1, v(w_{l+1}, w_l, b_{l+1}, b_l)), \quad (20)$$

$$v(w_{l+1}, w_l, b_{l+1}, b_l) = \frac{p(w_{l+1} \mid D, K, b_l)p(w_l \mid D, K, b_{l+1})}{p(w_l \mid D, K, b_l)p(w_{l+1} \mid D, K, b_{l+1})} \quad (21)$$

$$= \exp(n(b_{l+1} - b_l)(E_n(w_{l+1}) - E_n(w_l))), \quad (22)$$

where Eq. (20) ensures a detailed balance condition.

The main term $\tilde{F}_n(K, b_l)$ of $F_n(K, b_l)$ is calculated from an MCMC sample as follows:

$$\tilde{F}_n(K, b_l) = -\frac{1}{b_l} \log \prod_{l'=1}^{l-1} \frac{\tilde{Z}(K, b_{l'+1})}{\tilde{Z}(K, b_{l'})} \quad (23)$$

$$= -\frac{1}{b_l} \sum_{l'=1}^{l-1} \log \langle \exp(-n(b_{l'+1} - b_{l'})E_n(w_{l'})) \rangle_{b_{l'}}, \quad (24)$$

where $\langle \dots \rangle_b$ is approximated by the sample mean of an MCMC sample. The optimal values \hat{K} and \hat{b} , which minimize $F_n(K, b_l)$, are estimated as a grid search by using replicas as follows:

$$(\hat{K}, \hat{b}) = \arg \min_{K, b_l} F_n(K, b_l). \quad (25)$$

3. Demonstration

We demonstrated how efficient our framework is through simulation in which the same synthetic data as used by Nagata et al.⁶⁾ were used. The synthetic data $D = \{X_i, Y_i\}_{i=1}^n$ shown in Fig. 1 were generated from the true probability density as follows:

$$q(y | x, w_0, b_0) = \sqrt{\frac{b_0}{2\pi}} \exp\left(-\frac{b_0}{2}(y - f(x; w_0))^2\right), \quad (26)$$

where $b_0 > 0$ and $w_0 = \{a_k^*, \mu_k^*, \rho_k^*\}_{k=1}^{K_0}$ are respectively the true inverse noise variance and true parameter, as in Tables I and II. The inputs $\{X_i\}_{i=1}^n$ were linearly spaced between the interval $[X_1, X_n] = [0, 3]$ with the spectral resolution $\Delta x = 0.01$, where the number of samples was $n = 301$.

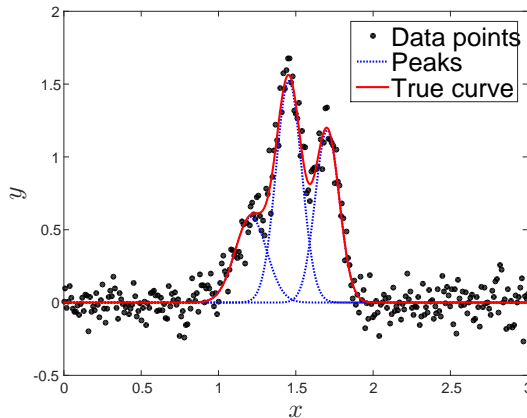


Fig. 1. (Color online) Synthetic data. Horizontal and vertical axes respectively represent input x and output y . Black dots show synthetic data $D = \{X_i, Y_i\}_{i=1}^n$. Red solid line and blue dotted ones respectively show true curve $y = f(x; w_0)$ and Gaussian peaks $y = \phi_k(x; \mu_k^*, \rho_k^*)$.

Table I. Number of peaks and inverse noise variance

	K	b
Estimated	3	1.06×10^2
True	3	10^2

In this simulation, the values $\{b_l\}_{l=2}^L$ were logarithmically spaced between the interval $[nb_2, nb_L] = [10^{-4}, 10^8]$, where the number of replicas was $L = 400$. The model size K was set as the natural numbers from 1 to 5. We also assumed the case in which there are no peaks in given data as $K = 0$ (see Appendix A). The hyperparameters were $\kappa = 1.7$, $\mu_0 = 1.5$,

Table II. Parameters of each Gaussian peak

		a_k	μ_k	ρ_k
Mode 1 ($k = 1$)	Estimated	0.5791 ± 0.0540	1.2568 ± 0.0390	52.8141 ± 18.5272
	True	0.587	1.210	95.689
Mode 2 ($k = 2$)	Estimated	1.3526 ± 0.1504	1.4605 ± 0.0042	176.1283 ± 28.5087
	True	1.522	1.455	146.837
Mode 3 ($k = 3$)	Estimated	1.1603 ± 0.0479	1.7032 ± 0.0043	150.6027 ± 14.8082
	True	1.183	1.703	164.469

$\alpha = 0.4$, and $\nu = 0.01$ in heuristics. The total MCMC sweeps were 100,000 including 50,000 burn-in sweeps: an MCMC sample w_l of size 50,000 for every b_l was obtained. The estimation results are listed in Tables I and II. The parameters of each Gaussian peak were estimated as the posterior mean with the posterior standard deviation for \hat{K} and \hat{b} .

First, we discuss how to estimate both noise variance and number of peaks. (A) Bayes free energy and (B) the posterior mean of the mean square error are shown in Fig. 2. The horizontal axes represent b in log scale. The colored solid lines show $F_n(K, b)$ for each K in (A) and $\langle E_n(w) \rangle_b$ for each K in (B). Three lines of $K \geq 3$ almost overlap in (A-1) and (B-1), whose enlarged views around the black circles are respectively (A-2) and (B-2). The markers in (A-2) and (B-2) indicate the grid points defined by $\{b_l\}_{l=1}^L$. The black solid lines in (B) show the function $1/2b$. The vertical black dashed lines and vertical black dash-dot ones respectively show the true value $b = b_0$ and estimated value $b = \hat{b}$. There is a minimum point of $F_n(b, K)$ depending on each value of K . The optimal values $(\hat{K}, \hat{b}) = (3, 1.06 \times 10^2)$ are estimated as shown in (A-2), where the true values are $(K_0, b_0) = (3, 10^2)$. This result is also interpreted probabilistically (see Appendix B). Strictly speaking, the value \hat{b} is not Bayes optimal in the true sense of the word. The point at the intersection of the purple solid line with the black solid line shown in (B-2) is truly optimal since Eq. (18) holds at this point. The estimation accuracy depends on the grid size defined by $\{b_l\}_{l=2}^L$. The gap between the truly optimal value of b and true value b_0 is a finite sample bias.

Second, we discuss the validity of our framework. The dependency on b in model selection is shown in Fig. 3. The horizontal axis represents b in log scale. The colored markers show the estimated model size \hat{K}_b , which minimize $F_n(K, b)$ for each b as follows:

$$\hat{K}_b = \arg \min_K F_n(K, b_l) \quad (27)$$

$$= \arg \min_K \tilde{F}_n(K, b_l). \quad (28)$$

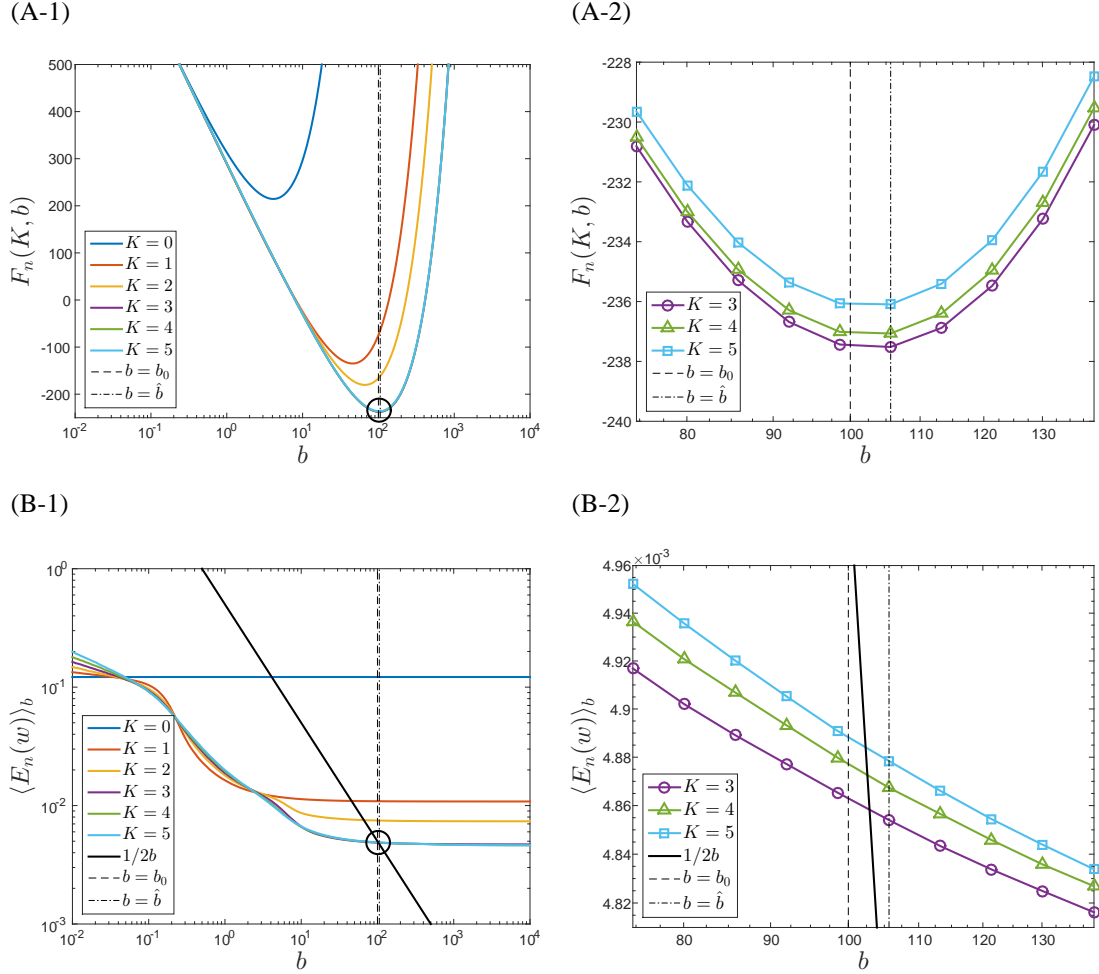


Fig. 2. (Color online) (A) Bayes free energy and (B) posterior mean of mean square error. Horizontal axes represent b in log scale. Colored solid lines show $F_n(K, b)$ for each K in (A) and $\langle E_n(w) \rangle_b$ for each K in (B). Three lines of $K \geq 3$ almost overlap in (A-1) and (B-1) whose enlarged views around black circles are respectively (A-2) and (B-2). Markers in (A-2) and (B-2) indicate grid points defined by $\{b_l\}_{l=1}^L$. Black solid lines in (B) show function $1/2b$. Vertical black dashed lines and vertical black dash-dot ones respectively show true value $b = b_0$ and estimated value $b = \hat{b}$.

Note that $\hat{K}_{b_0} = \arg \min_K \tilde{F}_n(K, b_0)$ is regarded as the optimal number of peaks in Nagata et al.'s framework.⁶⁾ The vertical black dashed lines and vertical black dash-dot ones respectively show the true value $b = b_0$ and estimated value $b = \hat{b}$. The estimated model size \hat{K}_b changes depending on the value of b , where there is a rough trend in which \hat{K}_b becomes larger as b increases. This trend is explained by the asymptotic form of $\tilde{F}_n(K, b)$. If the sample size n is sufficiently large, $\tilde{F}_n(K, b)$ is expressed as

$$\tilde{F}_n(K, b) = nE_n(w_0) + \frac{\lambda}{b} \log nb + \frac{1}{b} O_p(\log \log nb), \quad (29)$$

where w_0 is the parameter set that minimizes the Kullback-Leibler divergence of a statistical model from a true distribution, and $\lambda > 0$ is a rational number called the real log canonical threshold (RLCT).^{23,24)} The value of RLCT is determined by the pair of a statistical model and true distribution, and the ones determined by Eqs. (4) and (26) are clarified for several cases of (K, K_0) as $b = b_0$.²¹⁾ The values $E_n(w_0)$ and λ respectively become larger and smaller as K increases. The term $nE_n(w_0)$ dominantly works for model selection as large b : overfitting occurs. The term $\lambda \log nb$ dominantly works as small b : overpenalizing occurs. A moderate model is estimated under the moderate value of b . Estimating the optimal value of b is indispensable, and this result shows the validity of our framework.

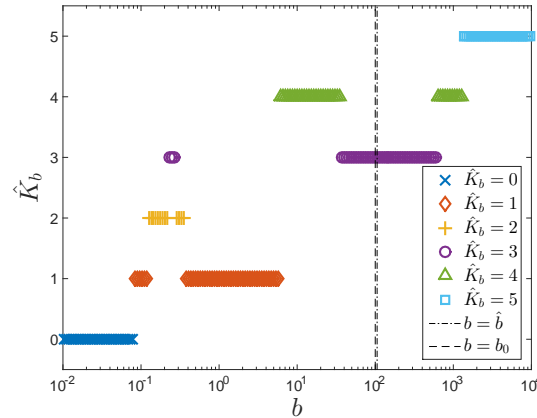


Fig. 3. (Color online) Dependency on noise variance in model selection. Horizontal axis represents b in log scale. Estimated model size \hat{K}_b , which minimizes $F_n(K, b)$ for each b , is plotted as colored marker. Vertical black dashed lines and vertical black dash-dot ones respectively show true value $b = b_0$ and estimated value $b = \hat{b}$.

Finally, we discuss the validity of our framework from another viewpoint. (A) Posterior mean of μ_k , (B) posterior standard deviation of μ_k , and (a-d) marginal posterior distribution of μ_k as $K = K_0 = 3$ are shown in Fig. 4. The horizontal axes in (A-B) represent b in log scale. The colored solid lines show the posterior mean of μ_k for each mode in (A) and twice the posterior standard deviation of μ_k for each mode in log scale in (B). The identification of $\{\mu_1, \mu_2, \mu_3\}$ is reassigned by sorting $\{\mu'_1, \mu'_2, \mu'_3\}$ at each MCMC sample w_l for every b_l in descending order in light of the exchange symmetry. The vertical black dashed lines and vertical black dash-dot ones respectively show the true value $b = b_0$ and estimated value $b = \hat{b}$. The horizontal black dotted lines show the true value μ_k^* for each mode in (A) and the spectral resolution Δx in (B). The vertical black solid lines in (A-B) correspond to each

value of b in (a-d). The histograms (a-d) of the MCMC samples $\{\mu_k\}_{k=1}^3$ for each b_l show the marginal posterior distribution of μ_k for each value of b as follows:

$$p(\mu_k | D, b) = \int \prod_{k=1}^3 da_k d\rho_k \prod_{k' \neq k} d\mu_{k'} p(w | D, K = 3, b), \quad (30)$$

where the coloring for each μ_k follows that in (A-B). The horizontal axes in (a-d) represent μ_k , and vertical ones represent frequency in log scale. The bin width was set as Δx as a physical constraint. The vertical black dotted lines in (a-d) show the true value μ_k^* for each mode, as in (A). The posterior mean of μ_k and posterior standard deviation of μ_k respectively change depending on b , where the changes in the support of posterior density correspond. These changes are drastic around $b = 10^1$, where each mean asymptotically approaches the true value μ^* from this region and each standard deviation monotonically decreases from the same region. The density of μ_1 , μ_2 , and μ_3 overlap and are non-identifiable if b is smaller than around 10^1 . If otherwise, they are separated and identifiable. Twice the standard deviation of μ_2 is smaller than Δx , as (c) $b = \hat{b}$: a kind of super-resolution. This effect is based on the same principle as super-resolution microscope techniques.^{25,26)} Twice the standard deviation of μ_1 , μ_2 , and μ_3 are also smaller than Δx , as (d) $b > \hat{b}$, whereas the support of μ_1 does not cover the true value μ_1^* : outside the confidence interval. An appropriate setting of b provides an appropriate precision of parameter estimation. Estimating the optimal value of b is indispensable even if the true model size K_0 is known; thus, this result also shows the validity of our framework.

4. Discussion and Conclusion

We constructed a framework that enables the dual estimation of noise variance and number of peaks and demonstrated the effectiveness of our framework through simulation. We also warned that there are the risks of overfitting, overpenalizing, and misunderstanding the precision of parameter estimation without the estimation of noise variance. Our framework is an extension of Nagata et al.s framework and is versatile and applicable to not only spectral deconvolution but also any other nonlinear regression with hierarchical statistical models.

Our framework is also considered as a learning scheme in radial basis function networks. However, the goal of spectral deconvolution is not to predict any future data, as the goal of most other learning tasks, but to identify the true model since spectral deconvolution is an inverse problem of physics. This is the reason we do not adopt Bayes generalization error but adopt Bayes free energy for hyperparameter optimization and model selection. The Akaike information criterion (AIC)²⁷⁾ and Bayesian information criterion (BIC),²⁸⁾ which are

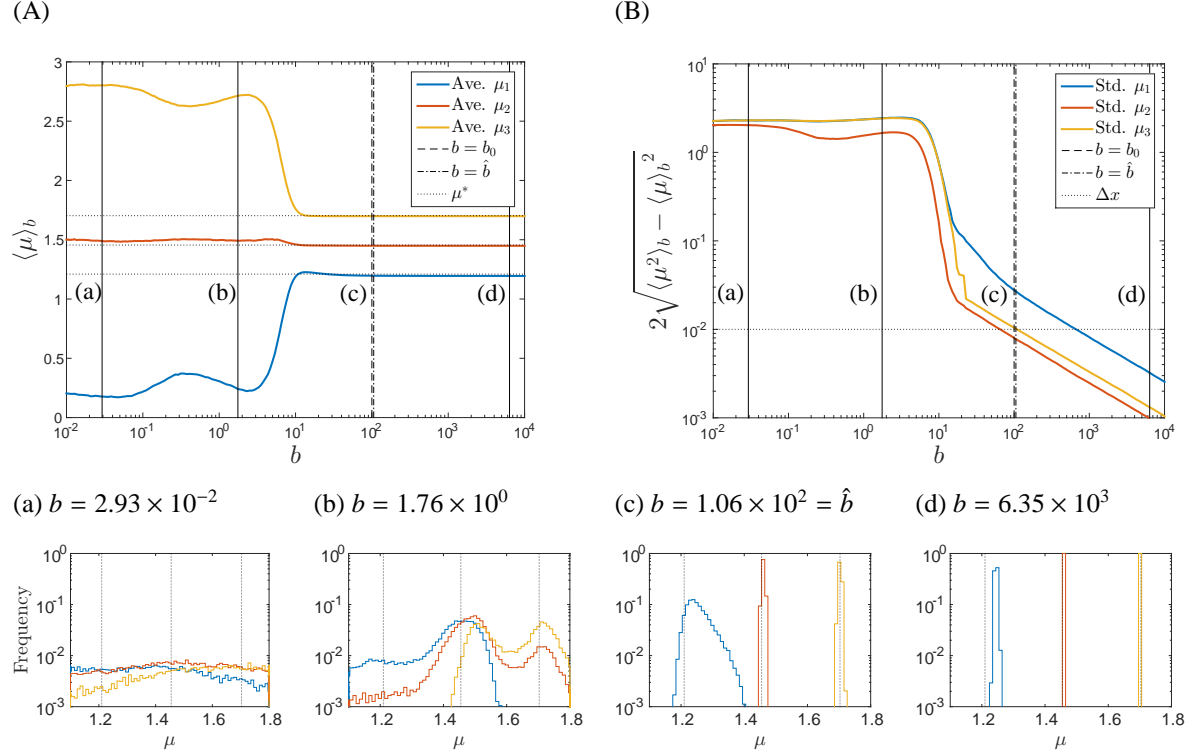


Fig. 4. (Color online) (A) Posterior mean of μ_k , (B) posterior standard deviation of μ_k , and (a-d) marginal posterior distribution of μ_k as $K = K_0 = 3$. Horizontal axes in (A-B) represent b in log scale. Colored solid lines show posterior mean of μ_k for each mode in (A) and twice posterior standard deviation of μ_k for each mode in log scale in (B). Vertical black dashed lines and vertical black dash-dot ones respectively show true value $b = b_0$ and estimated value $b = \hat{b}$. Horizontal black dotted lines show true value μ_k^* for each mode in (A) and Δx in (B). Vertical black solid lines in (A-B) correspond to each value of b in (a-d). Histograms (a-d) of MCMC samples μ_k for each b_l show marginal posterior distribution of μ_k for each b , where coloring for each μ_k follows that in (A-B). Horizontal axes in (a-d) represent μ_k , and vertical ones represent frequency in log scale. Vertical black dotted lines also show true value μ_k^* for each mode, as in (A).

respectively an approximation of the generalization error and Bayes free energy, do not hold for hierarchical models such as radial basis function networks: the widely applicable information criterion (WAIC)²⁹⁾ and widely applicable Bayesian information criterion (WBIC)³⁰⁾ generally hold for any statistical model. If noise variance is unknown, these criteria do not lead to computational reduction since the value of noise variance need to be estimated, as discussed in Sect. 3. The example we gave is classified as an unrealizable and singular (or regular) case,³¹⁾ which is a difficult problem. On the other hand, the example Nagata et al. gave⁶⁾ is classified as a realizable and singular (or regular) case, which is a relatively easy problem. Statistical hypothesis testing does not hold for a singular case. Our scheme is also valid and sophisticated from the viewpoint of statistics.

Acknowledgment

This work was partially supported by a Grant-in-Aid for Scientific Research on Innovative Areas (No. 25120009).

References

- 1) N. V. Tkachenko: *Optical spectroscopy: methods and instrumentations* (Elsevier, 2006).
- 2) G. C. Allen and R. F. McMeeking: *Analytica Chimica Acta* **103** (1978) 73.
- 3) R. Fischer and V. Dose: (2000).
- 4) S. G. Razul, W. Fitzgerald, and C. Andrieu: Nuclear Instruments and Methods in Physics Research Section A: Accelerators, Spectrometers, Detectors and Associated Equipment **497** (2003) 492.
- 5) A. Masson, L. Poisson, M.-A. Gaveau, B. Soep, J.-M. Mestdagh, V. Mazet, and F. Spiegelman: *The Journal of Chemical Physics* **133** (2010) 054307.
- 6) K. Nagata, S. Sugita, and M. Okada: *Neural Networks* **28** (2012) 82.
- 7) V. Mazet, S. Faisan, S. Awali, M.-A. Gaveau, and L. Poisson: *Signal Processing* **109** (2015) 193.
- 8) T. Kasai, K. Nagata, M. Okada, and T. Kigawa: *Journal of Physics: Conference Series*, Vol. 699, 2016, p. 012003.
- 9) P. Hong, H. Miyamoto, T. Niihara, S. Sugita, K. Nagata, et al.: *J Geol Geophys* **5** (2016) 2.
- 10) K. Hagino: *Phys. Rev. C* **93** (2016) 061601.
- 11) K. Hukushima and K. Nemoto: *Journal of the Physical Society of Japan* **65** (1996) 1604.
- 12) C. J. Geyer: (1991).
- 13) P. J. Green: *Biometrika* **82** (1995) 711.
- 14) A. Jasra, D. A. Stephens, and C. C. Holmes: *Biometrika* **94** (2007) 787.
- 15) B. Efron and C. Morris: *Journal of the American Statistical Association* **68** (1973) 117.
- 16) H. Akaike: *Trabajos de estadística y de investigación operativa* **31** (1980) 143.
- 17) D. J. MacKay: *Neural computation* **4** (1992) 415.
- 18) W. Demtröder: *Laser spectroscopy: basic concepts and instrumentation* (Springer Science & Business Media, 2013).
- 19) R. Loudon: *The quantum theory of light* (Oxford university press, 2000).
- 20) D. S. Broomhead and D. Lowe: *Radial basis functions, multi-variable functional interpolation and adaptive networks* (1988).

- 21) S. Tokuda, K. Nagata, and M. Okada: IPSJ Transactions on Mathematical Modeling and Its Applications **6** (2013) 117.
- 22) N. Metropolis, A. W. Rosenbluth, M. N. Rosenbluth, A. H. Teller, and E. Teller: The journal of chemical physics **21** (1953) 1087.
- 23) S. Watanabe: Neural Computation **13** (2001) 899.
- 24) S. Watanabe: *Algebraic geometry and statistical learning theory* (Cambridge University Press, 2009), Vol. 25.
- 25) E. Betzig: Optics letters **20** (1995) 237.
- 26) E. Betzig, G. H. Patterson, R. Sougrat, O. W. Lindwasser, S. Olenych, J. S. Bonifacino, M. W. Davidson, J. Lippincott-Schwartz, and H. F. Hess: Science **313** (2006) 1642.
- 27) H. Akaike: IEEE transactions on automatic control **19** (1974) 716.
- 28) G. Schwarz et al.: The annals of statistics **6** (1978) 461.
- 29) S. Watanabe: Neural Networks **23** (2010) 20.
- 30) S. Watanabe: The Journal of Machine Learning Research **14** (2013) 867.
- 31) S. Watanabe: Journal of Physics: Conference Series, Vol. 233, 2010, p. 012014.
- 32) A. Gelman, J. B. Carlin, H. S. Stern, and D. B. Rubin: *Bayesian data analysis* (Chapman & Hall/CRC Boca Raton, FL, USA, 2014), Vol. 2.
- 33) D. J. MacKay: Maximum entropy and Bayesian methods, 1996, pp. 43–59.

Appendix A: Bayes free energy for no-peaks model

We define the function $f(x; w = \phi) = 0$ as $K = 0$, where ϕ is the empty set. The statistical model of no-peaks spectrum and marginal likelihood are respectively as follows:

$$p(y | x, w = \phi, b) = \sqrt{\frac{b}{2\pi}} \exp\left(-\frac{b}{2}y^2\right), \quad (31)$$

$$Z_n(K = 0, b) = \prod_{i=1}^n p(Y_i | X_i, w = \phi, b) \quad (32)$$

$$= \left(\frac{b}{2\pi}\right)^{\frac{n}{2}} \exp(-nbE_n(w = \phi)), \quad (33)$$

$$E_n(w = \phi) = \frac{1}{2n} \sum_{i=1}^n Y_i^2, \quad (34)$$

where they correspond to Eqs. (4), (11), and (13). Bayes free energy and the posterior mean of mean square error are also respectively as follows:

$$F_n(K = 0, b) = nbE_n(w = \phi) - \frac{n}{2}(\log b - \log 2\pi), \quad (35)$$

$$\langle E_n(w = \phi) \rangle_b = E_n(w = \phi), \quad (36)$$

where they can be calculated without any MCMC scheme.

Appendix B: Hierarchical Bayes approach

In Sect. 3, we adopted the empirical Bayes (or type II maximum likelihood) approach,^{15–17)} in which K and b are estimated by minimization of $F_n(K, b)$ (or maximization of $Z_n(K, b)$). The hierarchical Bayes approach,³²⁾ which takes into account the posterior density of K and b , is also suitable for our framework. The prior density of K and b is set as $\varphi(K, b) = \varphi(K)\varphi(b)$, where $\varphi(K)$ is a discrete uniform distribution on the natural numbers $\{0, 1, 2, 3, 4, 5\}$, and $\varphi(b)$ is a continuous uniform distribution on the interval $[b_1, b_L]$. The joint posterior probability and marginal ones are expressed as

$$P(K, [b_l, b_{l+1}] \mid D) = \int_{b_l}^{b_{l+1}} db p(K, b \mid D), \quad (37)$$

$$p(K, b_l \mid D) = \frac{\exp(-F_n(K, b_l))}{\sum_{K=0}^5 \int_{b_1}^{b_L} db \exp(-F_n(K, b))}, \quad (38)$$

$$P(K \mid D) = \sum_{l=1}^{L-1} P(K, [b_l, b_{l+1}] \mid D), \quad (39)$$

$$P([b_l, b_{l+1}] \mid D) = \int_{b_l}^{b_{l+1}} db p(b \mid D), \quad (40)$$

$$p(b_l \mid D) = \sum_{K=0}^5 p(K, b_l \mid D), \quad (41)$$

where the integration along the b axis is calculated by the trapezoidal rule. The (A) joint probability of K and b , (B) marginal probability of K , (C) marginal probability of b , and (D) marginal probability density of b are shown in Fig. 5. The horizontal axes represent b in log scale. The colored stairstep graphs in (A) show the joint probability $P(K, [b_l, b_{l+1}] \mid D)$ for each K . Three graphs of $K < 3$ almost overlap in contrast to Fig. 2 (A-1). The black bar in (B) shows the marginal probability $P(K \mid D)$, black stairstep graph in (C) shows the marginal probability $P([b_l, b_{l+1}] \mid D)$, and black solid line in (D) shows the marginal probability density $p(b \mid D)$. The markers in (D) indicate the grid points defined by $\{b_l\}_{l=1}^L$. The vertical black dashed lines and vertical black dash-dot ones respectively show the true value $b = b_0$ and estimated value $b = \hat{b}$, as in Fig. 2. Both b_0 and \hat{b} are within the same interval of b , which maximize the probabilities $P(K, [b_l, b_{l+1}] \mid D)$ and $P([b_l, b_{l+1}] \mid D)$ in this case. Other optimal values of K and b , which respectively maximize $P(K \mid D)$ and $p(b \mid D)$, are the same as the optimal values \hat{K} and \hat{b} in this case. These values are not always consistent in practice, and

there is a continuous discussion: which is better, to optimize or to integrate out?³³⁾ The users of our framework can choose a better way in light of their perspective.

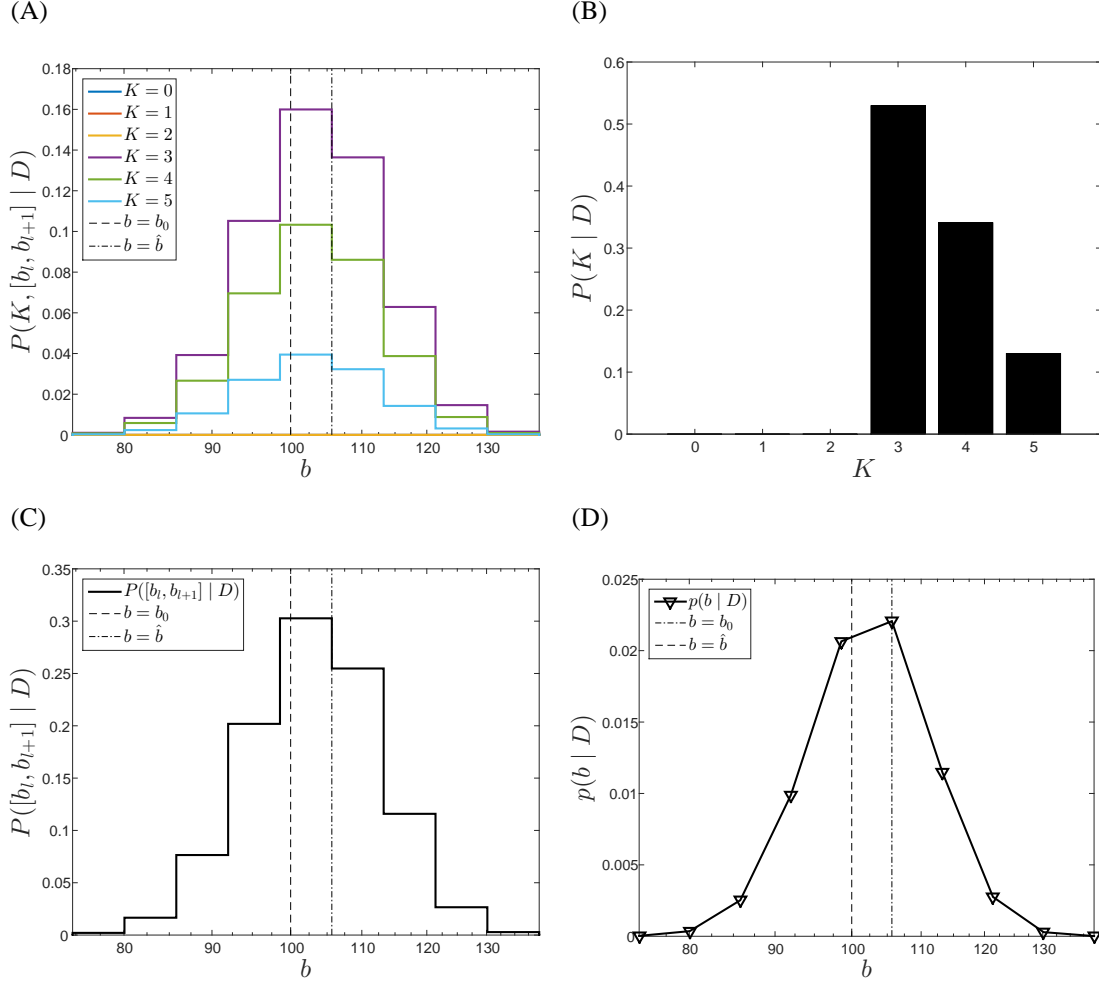


Fig. 5. (Color online) (A) Joint probability of K and b , (B) marginal probability of K , (C) marginal probability of b , and (D) marginal probability density of b . Horizontal axes represent b in log scale. Colored stairstep graphs in (A) show joint probability $P(K, [b_l, b_{l+1}] | D)$ for each K . Three graphs of $K < 3$ almost overlap in contrast to Fig. 2 (A-1). Black bar in (B) shows marginal probability $P(K | D)$, black stairstep graph in (C) shows the marginal probability $P([b_l, b_{l+1}] | D)$, and black solid line in (D) shows marginal probability density $p(b | D)$. Markers in (D) indicate grid points defined by $\{b_l\}_{l=1}^L$. Vertical black dashed lines and vertical black dash-dot ones respectively show true value $b = b_0$ and estimated value $b = \hat{b}$, as in Fig. 2.